BUILDING A PRACTICAL MOT FOR STUDENT RESEARCH

Bachelor Project

Exam's Number: xxxxxx
Flow Number: xx

Supervisors: Jan Arlt, Adam S. Chatterley

Department of Physics and Astronomy
Aarhus university
June 2024

Abstract

In this bachelor project, a magneto-optical trap (MOT) was constructed and characterized. This includes two laser optics boards, the magnetic coils, and the vacuum system. The MOT setup was supported by a LabVIEW program, which allows for easy controls. The setup makes it possible to both trap rubidium-87 atoms, as well as take both static and dynamic measurements on them. The goal was to make the setup practical and approachable for students for exercise experiments in the future. The construction of the MOT is described in detail, with calculations for the magnetic coils, and other relevant parts. In the appendix is a user manual for future use of the MOT.

Some initial data is then analysed to characterize the MOT. The MOT cools the rubidium atoms to approx. 0.10(5) mK. The optimal settings for the MOT were determined through static measurements. It is concluded that the MOT works well, and has succeeded in trapping rubidium-87 atoms, though it needs some adjusting for more precise temperature measurements. At the same time the setup is visually approachable for new students and relatively easy to maneuver.

Resumé (dansk)

I dette bachelor projekt, beskrives hvordan en magneto-optisk fælde (MOT) blev konstrueret og karakteriseret. Dette inkluderer to laseroptiske opstillinger, to magnetiske spoler, og et vakuumsystem. Et LabVIEW program blev implementeret for nem kontrol af MOT'en. Den samlede opstilling gør det muligt at fange rubidium-87 atomer, og samtidig tage statiske og dynamiske målinger på atomerne. Målet var at lave en opstilling der var praktisk og let tilgængelig for studerende til brug i studieeksperimenter i fremtiden. Konstrueringen af MOT'en er beskrevet i detaljer, med beregninger på det magnetiske felt, og andre relevante størrelser. I bilaget er der vedlagt en manual for MOT'en til fremtidig brug.

Målinger er taget med MOT'en og analyseret, for at karakterisere den. MOT'en køler rubidiumatomerne ned til omtrent 0.10(5) mK. De optimale indstillinger for MOT'en er blevet bestemt med statiske målinger. Det bliver konkluderet at MOT'en virker godt, og har med succes fanget og kølet rubidium-87 atomer, trods der mangler lidt justering for mere præcise målinger af temperaturen. Samtidig er opstillingen let tilgængelig for nye studerende og relativt nem at manøvrerer.

TABLE OF CONTENTS

1 Introduction 1

2 Theoretical background 2

2.1 Hyperfine structure of rubidium 2

2.2 Atom-light interaction 4

2.3 The Magneto-Optical Trap (MOT) 6

2.4 Doppler-free spectroscopy 8

2.5 B-field gradient 10

3 Experimental setup 11

3.1 Vacuum system 13

3.2 The laser board 14

3.3 The MOT board 17

3.4 Control panel and LabVIEW program 19

4 Data analysis 20

4.1 Optimal settings for trapping 21

4.2 Relative atom number 21

4.3 Different repumper transitions 22

4.4 Temperature 23

5 Results & Discussion 24

6 Conclusion 29

6.1 Outlook 30

References 31

Appendix: User Manuel 32

1 Introduction

Ultracold atomic physics examines the quantum mechanical properties of atoms at near zero temperatures. An essential part of trapping and cooling neutral atoms is the magneto-optical trap (MOT). A MOT uses six laser beams, sent in from each spatial direction, to trap and cool a sample of atoms in the intersection of the beams. The first MOTs were constructed in the mid 1980s, to cool and trap samples of up to 10^8 atoms [1]. Since then, MOTs have been used in various research within atomic physics, and is still widely used as the first step of many modern physics experiments on ultracold atoms. Recently, it has also found its use within the field of quantum computers. Here, a MOT is used to provide atoms to be used as Qubits in quantum computers, which is very relevant for future scaling of this technology [2].

The construction of a MOT requires a laser of a very specific frequency, slightly detuned from an atomic transition, specific for the atoms being trapped. Furthermore, a vacuum is needed inside the MOT, to limit random collisions that would increase the momentum of the atoms, thereby allowing the atoms to escape. Therefore, trapping a sample of atoms also requires control of the released sample into the vacuum chamber by dispensers.

The MOT described here, is built specifically with an aim to make it very approachable for physics students. My main focus was the design and construction of the optics setup and the magnetic field, making it visually clear, practical in size, and simple to use. My lab-partner's main focus was to implement a LabVIEW program, to control different parameters of the MOT. The MOT effectively trapped and cooled rubidium-87 atoms down below 1 mK temperatures, while allowing users to do multiple different experiments, both static and dynamic, on the trapped atoms. Initial measurements have been carried out, and used to characterize the MOT.

2 Theoretical background

In the following, the relevant theory for trapping rubidium-87 atoms with a MOT is described. The theory is general, but rubidium atoms are used as the main example, since they are used in our setup.

2.1 Hyperfine structure of rubidium

It is essential to know the atomic transitions of the atoms, in order to trap and cool them. Rubidium is the fifth alkali metal with one electron in its outer shell. Thereby, it has total electron spin of one half, $S = 1/2$, and the ground state has angular momentum of zero, $L = 0$, which leads to $J = 1/2$ due to Spin-Orbit coupling. The ground state in atomic physics notation is written as $5S_{1/2}$, and the first excited state with $L = 1$ has states $5P_{1/2}$ and $5P_{3/2}$, with $J = 1/2$ and $J = 3/2$. It is the $5P_{3/2}$ state that is important for our trapping process, and is the state with the lowest energy of the two [3]. The nuclear spin for rubidium is $I = 3/2$, and so this leads to a set of hyper-fine splittings. For the ground state we denote the new states $F = I \pm J = 1$ *and* 2, and for the relevant first excited state, $5P_{3/2}$, we denote the states $F' = I \pm J = 0, 1, 2$ *and* 3. There are four F' states since all integer steps in-between the difference and the sum of I and J correspond to real states. These relevant states are shown in fig. 1. All transitions between the ground state and the relevant first excited state can now be written as $F = x \rightarrow F' = y$. Note that $F = x \rightarrow F = y$ or $F' = x \rightarrow F' = y$, is forbidden, because the selection rules in the dipole approximation force us to have $\Delta L = \pm 1$ [4]. Two specific transitions are shown in fig. 1, which are the transitions relevant for trapping rubidium in our setup.

The relative frequencies between the states in fig. 1 are not constant in an external B-field, due to the Zeeman effect. The atomic states are further divided into M_F eigenstates, and in a weak external magnetic field, the Zeeman splitting is given by

$$E = g_F \mu_B B M_F, \tag{1}$$

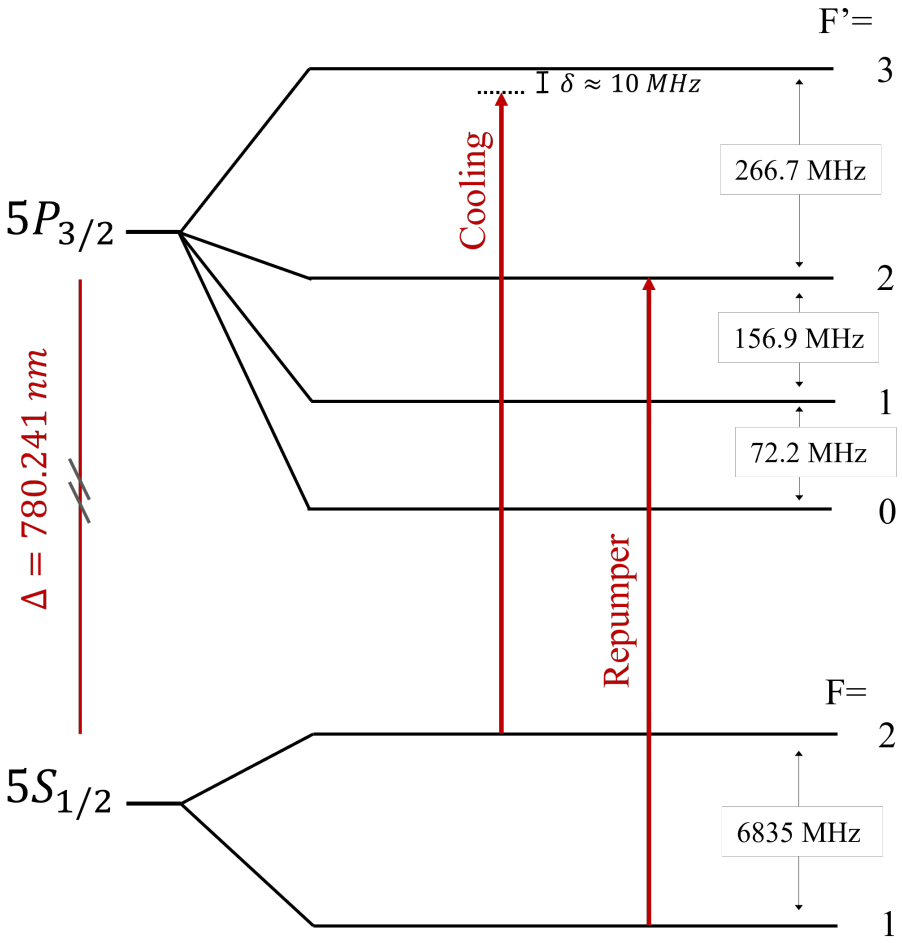

Figure 1: Transitions in rubidium-87. The marked transitions are the ones used in our experiment for the repumper and the cooling laser. Data from [3]. The detuning $\delta = \omega - \omega_0$ has a value in range $\delta = 12 \pm 10$ MHz in our experiments.

where g_F is the Landé g-factor, μ_B is Bohr-magneton, B is the size of the external field, and M_F is the quantum number for the specific eigenstate [4]. This implies the different eigenstates are perturbed differently, and so the relative frequency of a given transition is changed in the presence of an external magnetic field. The Zeeman effect is essential to a MOT, since it influences the atomic transitions, and thus the detuning, as described in the following section.

2.2 Atom-light interaction

Here, the interaction of light with an atom in a two-level system is described. This interaction is essential for how optical trapping is realised in a MOT.

Let $|g\rangle$ denote an F state in rubidium-87 and $|e\rangle$ denote an F' state. Let ω_0 be the difference in frequency for the $F = g \rightarrow F' = e$ transition. We apply an external electric field of monochromatic radiation, in our case a laser beam, with frequency ω, the detuning is then $\delta = \omega - \omega_0$. The Schrodinger equation is

$$i\hbar \frac{\partial \Psi(\mathbf{r}, t)}{\partial t} = \hat{H}\Psi(\mathbf{r}, t), \tag{2}$$

with the associated wave function given by

$$\Psi(\mathbf{r}, t) = c_g(t)\,|g\rangle + c_e(t)\,|e\rangle\, e^{-i\omega t}. \tag{3}$$

This choice of notation and the following derivation is inspired by the lecture notes of M. P. A. Jones [5] and the Atomic Physics book by Foot [4]. The perturbation due to the electric field is denoted as $V = \hat{d} \cdot \hat{E}$, where $\hat{d}$ is the dipole moment of the transition and $\hat{E}$ is the electric field with a polarization $\hat{\epsilon}$. The associated Rabi frequency Ω, for a plane wave $\hat{E}$, becomes

$$\Omega = \frac{E_0 \,\langle g|\, \hat{d} \cdot \hat{\epsilon}\, |e\rangle}{\hbar}. \tag{4}$$

The matrix element in eq. (4) is where the selection rules for a dipole approximation naturally present themselves. The matrix element is zero for certain so called forbidden transitions. The selection rules for the above conditions are $\Delta L = \pm 1, \Delta F = 0, \pm 1, \Delta M_F = 0, \pm 1$. For circular polarized light, $\Delta M_F = 0$ becomes a forbidden transition [4].

The evolution of the atom over time, depends primarily on the detuning and the Rabi frequency [5]. Using the rotating wave approximation, the probability of exciting the atom to $|e\rangle$ is

$$|c_e|^2 = \frac{\Omega}{\Omega'} \sin^2(\frac{\Omega' t}{2}), \tag{5}$$

where $\Omega' = \sqrt{\Omega^2 + \delta^2}$ [5]. Over time, the atom will shift between the excited state and the ground state due to the interaction with the laser. Until now, spontaneous emissions have been ignored, but are also important. Changing to Bloch formalism, spontaneous emissions with the rate Γ for the specific transition, can be implemented, and a relevant result to derive is the photon scattering rate R_{scatt}. The photon scattering rate is given by

$$R_{scatt} = \Gamma/2 \frac{I/I_{sat}}{1 + I/I_{sat} + 4\delta^2/\Gamma^2}, \tag{6}$$

where I is the electric field intensity, or specifically the laser intensity, and I_{sat} is the saturation intensity given by $I_{sat} = \frac{2\pi^2\hbar\Gamma c}{3\lambda^3}$ [4]. Importantly, we can now calculate the associated scattering force, F_{scatt}, for the photons "pushing" the atom as it interacts with them. This force can be calculated directly from the scattering rate R. Letting the photons have momentum $\hbar k$,

$$F_{scatt} = \hbar k \cdot \Gamma/2 \frac{I/I_{sat}}{1 + I/I_{sat} + 4\delta^2/\Gamma^2}. \tag{7}$$

This equation illustrates the very idea behind "pushing" atoms backwards by laser beams, and thereby trapping them. Here, when an atom is moving towards a laser, it experiences a force F_{scatt} in the opposite direction, from the absorption and re-emission of photons. F_{scatt} depends on the detuning, and so Zeeman splitting is important, as an external B-field will change the frequency of the atomic states and thereby change ω_0, and thus change the detuning. Therefore, if a sample of rubidium atoms is placed in a non-uniform B-field with a laser, and the laser frequency ω is adjusted accordingly, the atoms will be "pushed" by the laser when they experience a Zeeman shift, but are not "pushed" when they are at a zero B-field center. For atoms moving towards the laser, the detuning is also Doppler shifted due to the velocity of the atoms. The actual detuning should then be written as $\delta = \omega - \omega_0 + vk$ [4]. The final detuning therefore depends both on the velocity of any given atom, due to the Doppler shift, and the position for that atom in the magnetic field. How the Zeeman effect is used for trapping atoms in a MOT, is described in section 2.3.

With eq. (7) another key result can also be derived: The Doppler cooling limit. This limit, T_D, is the lowest temperature that can be achieved by laser cooling directly and it is given by $T_D = \hbar\Gamma/2k_b$ [4]. In practice, it is possible to achieve temperatures below this limit, for specifically tailored setups, but this is not explained within the two-level system interaction described here. For rubidium-87 with the transition we use, $F = 2 \rightarrow F' = 3$, T_D is approx. 146 µK, calculated with data from [3].

2.3 The Magneto-Optical Trap (MOT)

A MOT allows the user to trap a sample of atoms. In our setup there is a glass cell with a vacuum, where a small sample of rubidium is released into. A magnetic field is applied, with zero field in the center of the cell. A cooling laser is split into six laser beams and are sent into the glass cell, hitting the center where the field is zero, but the magnetic gradient is non-zero. The six beams are in counter-propagating pairs, and each pair is orthogonal to each other pair, as shown in fig. 2.

The cooling laser is set to match a certain transition in rubidium-87, $F = 2 \rightarrow F' = 3$ in our case, though slightly detuned from that exact transition. When atoms are travelling towards one of the beams, the change in the magnetic field causes a Zeeman shift for the transitions in the atoms. Furthermore, the atoms have a non-zero velocities, which means the detuning is also Doppler shifted. Due to these effects, though the Zeeman shift dominates in a MOT, the transition becomes resonant with the chosen cooling laser frequency, so the atoms are now absorbing photons from that beam and are "pushed" backwards by the photon scattering force. Thereby, the MOT slows down the atoms similarly for all six beams, thus decreasing the temperature of the atoms and trapping them in the center, where the B-field is zero and all the laser beams cross.

The polarization is very important as well. Assume that an atom is moving in the positive x-direction in fig. 2, and for now ignore the y- and z-direction. We need to make sure it is primarily the beam going in the negative x-direction that "pushes" the atom, so it ends up in the center again. This is done by polarization. Each beam is

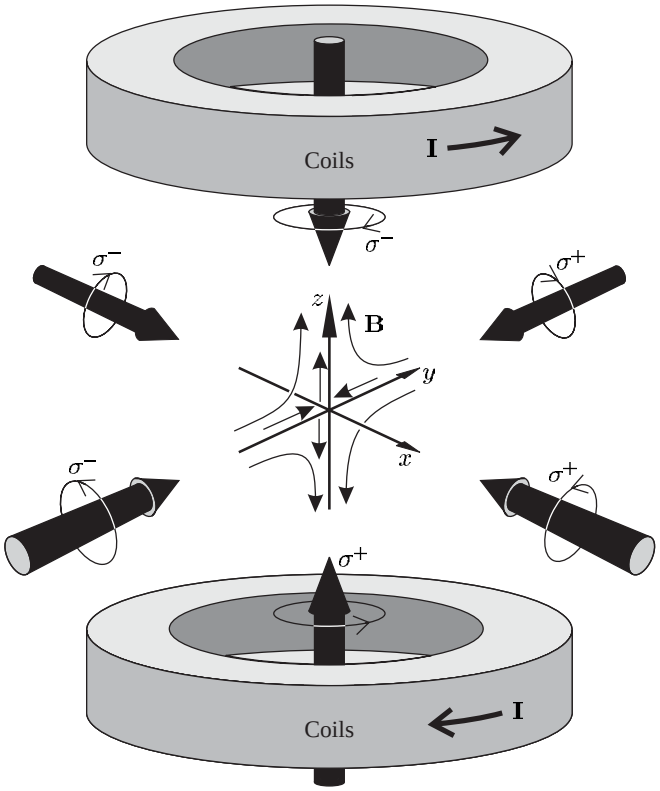

Figure 2: Illustration from Foot page 192 [4]. A pair of anti parallel coils, with six beams in anti-propagating pairs with opposite circular polarization.

sent in with circular-polarization, and, for each pair, one beam will have σ^+ and the other have σ^- polarization. For this example, a σ^+ laser beam is moving anti-parallel to the atom, and a σ^- beam is moving parallel to the atom. From the dipole selection rules, the σ^+ beam can only excite atoms from a state M_F to $M'_F = M_F + 1$ and σ^- only excites to $M'_F = M_F - 1$ [4]. The Zeeman shift decreases the energy for the $M'_F = M_F + 1$ for the atom in the positive x-direction, the σ^+ side, so an atom moving in this direction can easily absorb photons from the σ^+ beam. At the same time the $M'_F = M_F - 1$ state has increased in energy on this side, so the σ^- beam cannot excite the atom. This essentially makes sure atoms moving to one side are only "pushed" by the laser coming in towards them from that side, so they are slowed down and re-centered.

An important issue is that approx. 1 in every 1000 atoms that are excited from the $F = 2$ ground state, decays to $F = 1$ ground state instead of back to the $F = 2$ state [6]. Therefore, all atoms would in time decay to the $F = 1$ ground state, and the cooling laser would no longer be able to excite the atoms, and there could be no trapping. To adjust for this innate probability, a second laser is added: The repumper. The repumper is locked to a different transition, specifically the $F = 1 \rightarrow F' = 2$. The repumper excites atoms to the $F' = 2$ state, where the atoms can decay to the $F = 2$ state. This second laser has then effectively "repumped" the $F = 2$ state, and the cooling can continue. The intensity of the repumper does not need to be very large compared to the intensity of the cooling laser, since only a small fraction of atoms decay to the $F = 1$ ground state.

2.4 Doppler-free spectroscopy

Spectroscopy is used, to make sure both the cooling laser and the repumper, are actually at the right frequency. The lasers are sent trough another sample of rubidium first, in room temperature, and a photodiode measures the transmitted light. With the spectroscopy signal output, the lasers can be locked to a specific transition, and only produce light of that frequency. There is however a problem with sending light through a sample of rubidium to get the spectrum: the signal gets Doppler broadened. In general, the transition frequencies of different atoms in the sample are Doppler shifted due to those atoms' velocity by an amount vk, so the atoms absorb the laser emitted photons exactly when $\delta = \omega - \omega_0 = vk$. For a room temperature T and an atomic mass of rubidium-87 M, the most probable speed for a sample of rubidium is

$$u = \sqrt{2k_B T/M}, \tag{8}$$

where k_B is Boltzmann's constant [4]. Following the derivation in Foot [4], the full width at half maximum (FWHM), $\Delta\omega_D$, is given by

$$\Delta\omega_D = 2\sqrt{\ln(2)}\ \frac{u\omega_0}{c}, \tag{9}$$

where c is the speed of light. Evaluating eq. (9) at our lab, with $T = 19°\text{C}$, using the known constants, and the frequency ω_0 for the $F = 2 \rightarrow F' = 3$ rubidium-87 transition, the width becomes approx. $\Delta\omega_D = 420$ MHz. To compare, the difference between the $F' = 0$ and the $F' = 3$ is just below 500 MHz [3], so the Doppler broadening effect would make it nearly impossible to get a clear spectroscopy signal for the hyperfine splitting, and thereby extremely hard to lock the lasers to a specific peak.

Yet Doppler-free spectroscopy can be achieved through different methods to overcome this obstacle. The relevant method used in our setup is saturated absorption spectroscopy. In this method, a laser beam is split by a polarizing beam splitter (PBS) into a high intensity pump beam and a low intensity probe beam. Both beams are sent through a sample of rubidium from each side. Without the pump beam, the probe beam will simply pass through a sample of atoms, which will absorb light near a specific frequency. Due to Doppler broadening, the output signal for a photodiode measuring the probe beam has a large "valley" where light is absorbed. If a powerful pump beam is sent in the other way, all atoms with a rubidium transition close to that of the laser frequency (atoms with $v = 0$) have saturated. When saturated, the atoms cannot absorb any more light, so a "hole" is created, which the probe beam can "move through". The probe beam still creates the same overall "valley" shape since atoms with velocities very different from zero are only affected by one of the beams, not both. However, the probe beam signal will now have one or more peaks inside the "valley" due to the specific transitions in rubidium, that were saturated by the pump beam[4]. An example of the final output is shown in fig. 3.

Another interesting consequence of saturated absorption spectroscopy is the cross-resonant peaks, which are also visible in fig. 3. These peaks appear when a "hole" burnt by the pump beam, e.g. at a transition $F = 2 \rightarrow F' = 1$, reduces the absorption for the probe beam at the $F = 2 \rightarrow F' = 3$ transition due to different Doppler shifts [4]. This creates a cross-resonant peak exactly between the two transitions, so in this example the cross resonant peak would be denoted $F = 2 \rightarrow F' = 1, 3$.

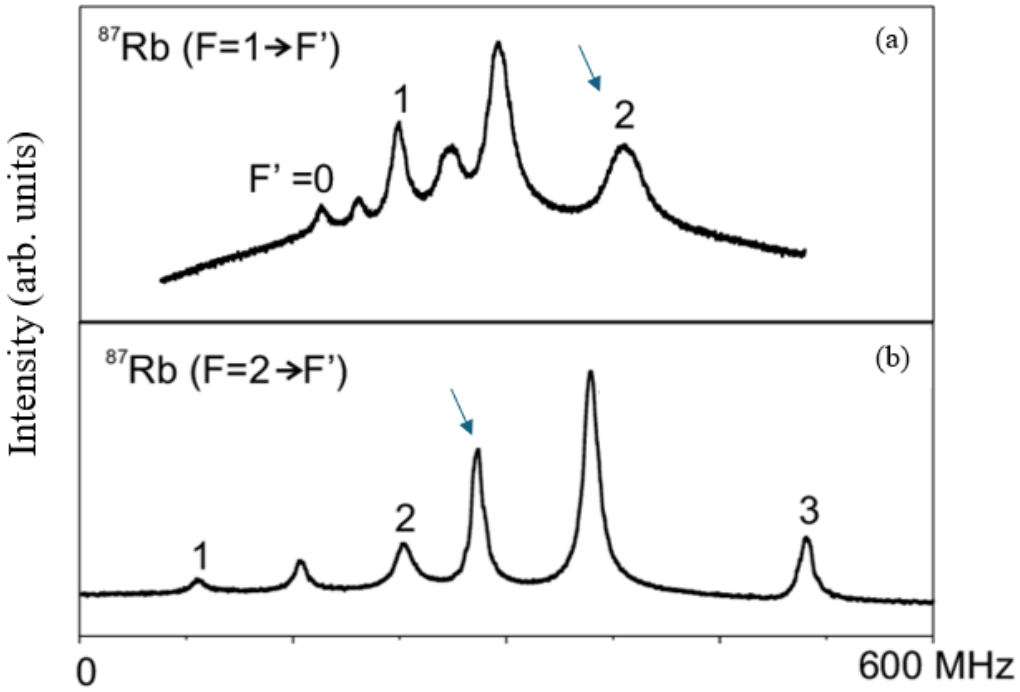

Figure 3: Saturated absorption spectra of the hyperfine structure of Rubidium 87 for the $5S_{1/2}$ to $5P_{3/2}$ transitions. Both with the exact transition marked, that is used to lock the associated laser. (a) Spectrum used for the repumper. (b) Spectrum used for the cooling laser. The figure is adjusted, though originally from [7].

In our setup, we actually lock the cooling laser to one of these cross resonant peaks, the $F = 2 \rightarrow F' = 1, 3$, the arrow in fig. 3 (b), because its peak is larger, and therefore easier to lock to. Afterwards, the frequency is increased, so the cooling laser frequency ends up approx. -10 MHz detuned below the $F = 2 \rightarrow F' = 3$ transition.

2.5 B-field gradient

When constructing a MOT, the B-field is essential, to give rise to the Zeeman splitting. Two coils are placed anti-parallel to one another, so the field is zero in the center, but the gradient is non-zero. The magnetic field needs a gradient of approximately 10-15 G/cm in the vertical direction through the coils for the MOT to work effectively [6]. In the following, the formula for the B-field gradient through a set of anti-parallel coils

is derived. Generally, the B-field above the center of a coil, at a distance z along the vertical axis through the center, is given by

$$B = \frac{\mu_0 N I}{2} \cdot \frac{R^2}{(R^2 + z^2)^{3/2}},$$

with R being the radius of the coil, with N turns and the current I, and μ_0 as the magnetic permeability [8]. The gradient then becomes

$$\frac{dB}{dz} = \frac{\mu_0 N I}{2} \cdot \frac{R^2 \cdot (-3z)}{(R^2 + z^2)^{5/2}}.$$

Add another coil, anti-parallel to the first, at a distance L above it, and evaluate at a distance L/2 in between both coils. Note this gives a factor of two, since both coils contribute to the gradient equally at the center. Thereby, we reach

$$\frac{dB}{dz}|_{z=L/2} = -\frac{3\mu_0 N I}{2} \cdot \frac{R^2 L}{(R^2 + L^2/4)^{5/2}}. \tag{10}$$

The minus sign just depends on the direction of the current. Note that eq. (10) only gives the gradient along the vertical axis, the z-axis in fig. 2, evaluated in the center. It can be shown that the gradient in x, y plane in fig. 2, is half the gradient of eq. (10), with opposite sign [4]. Now eq. (10) provides some spacial restrictions, which are important for constructing the coils.

3 Experimental setup

The final setup is shown in fig. 4. It consists of a laser control panel, two oscilloscopes used for laser locking, the vacuum system, and two separate optics boards. The optics boards are illustrated in fig. 6 and fig. 7. The laser board includes the lasers, the spectroscopy, and the fibre coupling, and is connected to the laser control panel. The MOT board contains the optical components for the actual trapping of rubidium. In the following subsections, different parts of the final setup are described. This includes the vacuum system, the laser board, the MOT board, and the control panel

and LabVIEW program. The laser board was already built to some extent, before this bachelor project commenced. The main credit for the construction of this optics board goes to Pablo Marulanda and Morten Strøe.

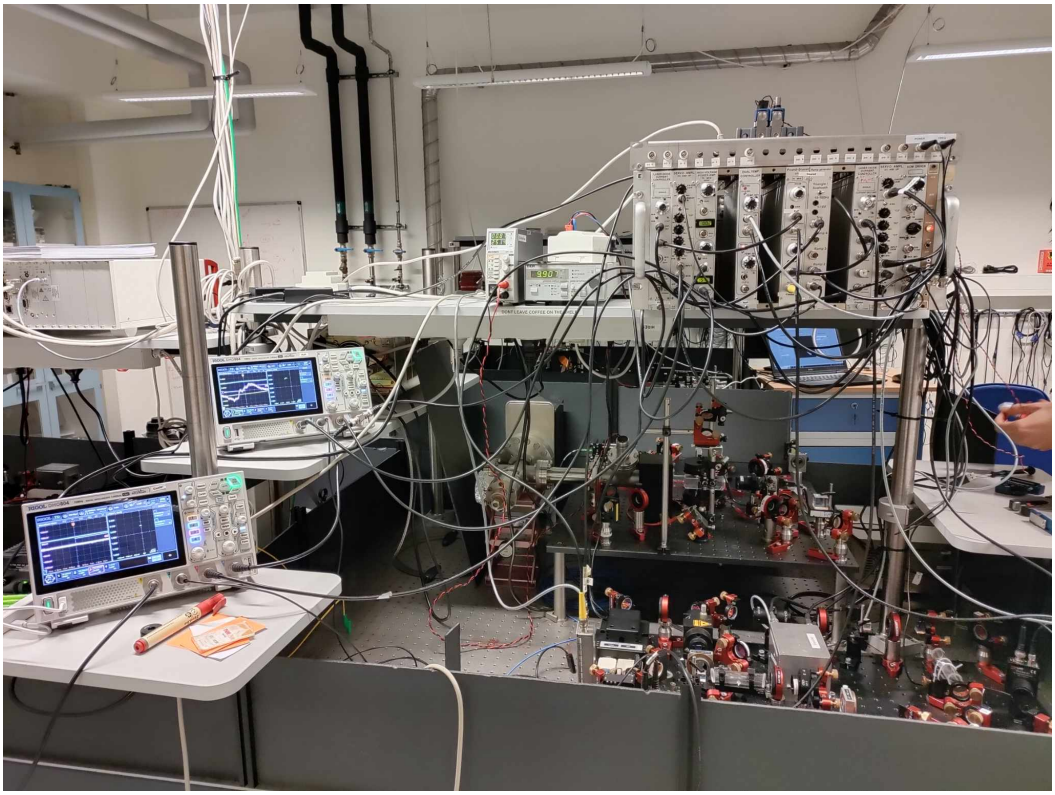

Figure 4: Current setup consisting of a control panel for the lasers (top right), two oscilloscopes used for laser locking (left), and the two optics boards: the laser board (bottom right) and the MOT board (center right). The vacuum setup is placed to the left of the MOT board (center).

So far, the setup has already been used by multiple master students on the Aarhus University course "Advanced Exercises in Experimental Physics". These students were asked to do static measurements with our MOT as an exercise. Within 20 minutes, they understood the setup and could manoeuvre it themselves and collect the data they needed. This included locking the lasers themselves and taking their measurements through the LabVIEW program. For future use, it is necessary for students to know how to operate the MOT. In the appendix, the laser locking procedure and the LabVIEW controls are described, so it is approachable for students to take data with this setup.

3.1 Vacuum system

To realise a MOT, it is necessary to limit the possibility of random collisions, which increases the momentum of the rubidium atoms. Therefore, a vacuum is needed inside the glass cell. The MOT's optimal conditions are at a pressure of approx. $10^{-8} - 10^{-9}$ mBar or lower [6]. To achieve this, the first task of this project consisted of constructing the vacuum system, shown in fig. 5.

The vacuum system consists of a glass cell, in which the MOT is realised, vacuum pumps to achieve a vacuum inside the chamber, dispensers for releasing the rubidium sample, and a mirror for visuals of the MOT with an IR-viewer. The vacuum chamber refers to the inside of the construction. Using the letters from fig. 5, a valve is placed at position C. Here, the first two vacuum pumps were connected to the system, to initially empty out the vacuum chamber. Afterwards, these pumps were disconnected. Position E is the ion-pump, which consistently keeps the pressure down. The glass cell is placed in-between the coils, at position A.

The vacuum system was constructed as follows. Initially the setup consisted of the valve, the glass window, an ion-pump, an empty dispenser-holder, and a blank flange, where the glass cell would later go. With this setup, the pumps were tested, and the setup tested for leakage. Initial testing showed no leakage in our setup. The next thing to do was to mount the dispensers. Three small dispensers of type RB/NF/7/25 FT10+10 were mounted and connected to a small power-supply. The mounted dispensers were placed in the dispenser-holder denoted B in fig. 5. Additionally, for storage purposes, seven of these small dispensers were placed in an aluminium pouch inside the vacuum system. Once the glass cell was mounted, the pumps were turned on, but the final pressure did not drop below 10^{-7} mBar. A small crack was found in the glass cell and fixed with 'Vacseal High Vacuum Leak Sealant'.

Each time a vacuum had to be achieved starting from atmospheric pressure, a combination of three different vacuum pumps were needed. After using the first two pumps, the pressure inside the chamber went down to 10^{-7} mBar, but plateaued there.

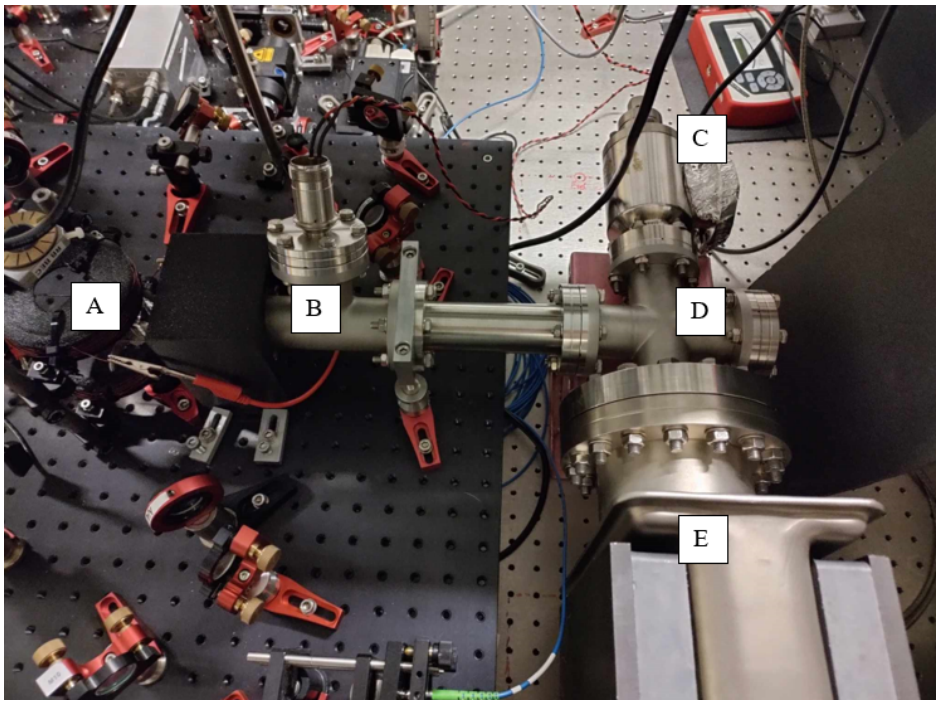

Figure 5: The vacuum system. A: The glass cell in-between the coils. B: The rubidium dispenser. C: A now empty mounting for the first and second pump, and a valve to close them off. D: A mirror to the right of the intersection for visual aid. An IR-viewer captures the MOT nicely through the mirror. E: The ion pump (the third, and permanent, pump).

Then, the third pump, the ion-pump, was turned on. Within a couple of days, the pressure went down to $5 \cdot 10^{-9}$ mBar. Once this final pressure was reached, the valve was closed and the first and second pump were disconnected. A little aluminium foil was placed on the empty mount to avoid dust. The ion-pump works by ionizing leftover atoms and molecules in the chamber, and uses an electric field to accelerate them onto its inner wall. For this procedure, the pressure must already be very low. The ion-pump has sustained a stable pressure of approx. $2(2)10^{-9}$ mBar, though it fluctuates slightly. Between position A and B in fig. 5 there is a black casing, specifically 3D-printed to protect the fragile glass cell, where the cell is mounted to the rest of the setup.

3.2 The laser board

The final laser board is shown in fig. 6. Here, the two laser beams are are prepared through spectroscopy. They are both split by a polarizing beam splitter (PBS), and

only a small fraction of the power of each laser is sent though their respective glass cells for spectroscopy. The splitting is controlled by $\lambda/2$-plates, which are used to turn the linear polarization of the beams. The main power of each laser beams is sent to the fibre coupler. The cooling laser light is detuned before reaching the fibre coupler, by passing through the acousto-optic modulator (AOM), which slightly changes the frequency of the light. The laser light sent through the glass cells is used for the saturated absorption spectroscopy, and then sent into two different photodiodes for each laser. One of the photodiodes is connected to an oscilloscope, allowing us to see the spectra for that laser beam, the other photodiode sends a feedback signal to associated laser. The feedback signals are used for locking the lasers. The lasers can be locked to the right frequency using the control panel. When the lasers are out-coupled on the MOT board, the light is already at the right frequency, and can be used to realise a MOT.

The laser board was already built to some extent prior to this project. However, some changes were made. The previous AOM used for detuning the cooling laser-light was swapped to a 100 MHz AOM, which is more practical for the transitions used. The alignment had to be redone to achieve as high an efficiency as possible. There was too much laser light travelling backwards through the setup. Therefore, the isolator for the cooling laser was swapped for a different one, that provided an order of magnitude better isolation. For the repumper, an extra isolator was placed for a more stable laser signal. Both lasers are ECDLs (external cavity diode lasers). The repumper is homemade, and can be relatively unstable. The cooling laser is a newer mini ECDL, and is generally more stable and easier to lock.

Once the setup was well aligned with a high efficiency, it was time for fibre-coupling. To send a laser through a fibre, that laser will have to hit a fibre core with a diameter of just five micrometres. The laser width was measured to be approx. 1350 micrometres in diameter, so a lens were used to focus the beam down. A focal length was calculated

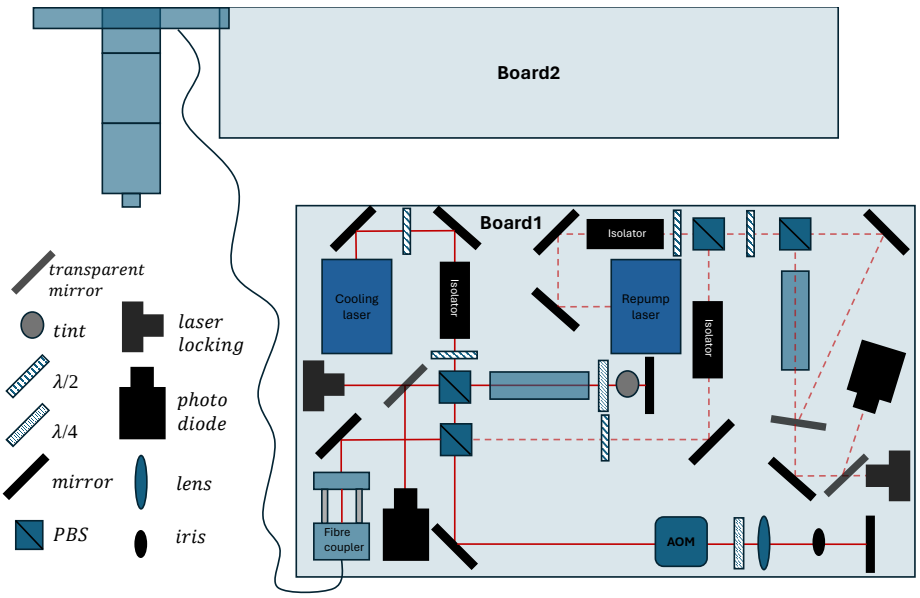

Figure 6: Illustration of the laser board, where the spectroscopy of both lasers take place. The illustration is seen from the same side as the picture of fig. 4 is taken. Illustration is not to scale.

using Svelto's eq. [9], given by

$$d(z) = d_0\sqrt{1 + (z/z_r)^2}, \quad z_r = \frac{\pi d_0^2}{4\lambda}, \tag{11}$$

where d(z) is the beam diameter at the focal length z away from the fibre, d_0 is the fibre core diameter and λ is the wavelength of the laser, which is approx. 780 nm. I rewrote the equation as

$$z = z_r\sqrt{(d(z)/d_0)^2 - 1}, \tag{12}$$

and calculated the focal length to be 6.8 mm. The closest lens available was a 6.24 mm lens. After aligning everything, the power output of the fibre for the cooling laser was approx. 19 mW, with 24 mW right before the fibre. So, approx. 80% efficiency in the fibre-coupling, which is relatively high. The repumper was then aligned such that only 3 mW came out the fibre. This is to make sure the repumper is significantly weaker than the cooling laser.

3.3 The MOT board

The MOT board, shown in fig. 7, contains the optical components around the glass cell where the atoms are captured. In our MOT, the cooling laser light is initially split into three arms, where each arm sends a beam into the MOT and then the light hits a mirror on the other side, effectively creating two beams for each arm. To divide the cooling light into three arms, it is split twice by PBSs. Both times, a $\lambda/2$-plate is placed before the PBS, allowing us to change the power in each arm. Thus, an equal laser power in each arm can be achieved. In each arm, $\lambda/4$-plates convert the linearly polarized cooling light into circular polarization, which is necessary for the MOT to work as described in section 2.3. A hole is cut near the middle of the MOT board, where the vertical laser goes downwards through the cell. One of the back-reflecting mirrors, and the associated $\lambda/4$-plate, is mounted underneath the board and placed below the hole.

The cooling laser beam needs a relatively large diameter for the experiment, to ensure a large area of intersection between the laser beams. Therefore, using eq. (12), a focal length of 7.0 cm was chosen for the out-coupling such that the final beam diameter would be 1.4 cm. The reason for this specific size is that the diameter of the mirrors is 2.5 cm, so hitting them at an angle of maximum 45 degrees means the effective size of the mirror can be as small as only $2.5\text{cm} \cdot \sin(45^o) = 1.77\text{cm}$. So choosing a 1.4 cm diameter, the beam is relatively large, but is not "clipped" within the optics setup, as light is not dumped on the edges of mirror-mounts.

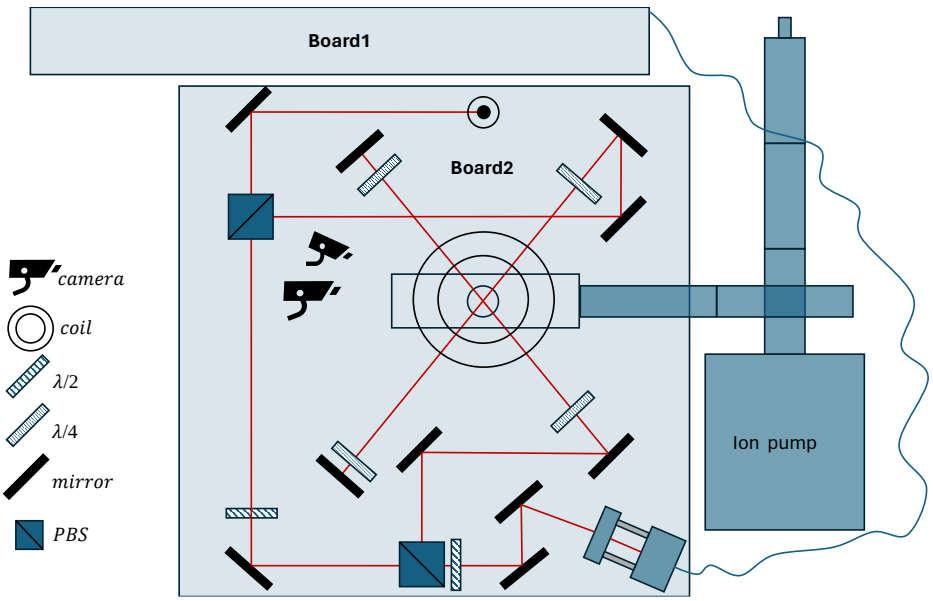

Figure 7: Illustration of the MOT optics board, where the trapping takes place, and the glass cell is placed as the square in the middle. The illustration is seen from the opposite side to where the picture in fig. 4 is taken. At the top of the board, the laser beam is sent vertically out of the page, to then go down through the cell from above. Illustration is not to scale.

The 19 mW cooling laser-power out the fibre loses another roughly 40% on the MOT optics board, so the power of each of the three laser arms is approx. 4 mW before hitting the cell. The repumper light is sent through the same fibre, and due to its orthogonal polarization it primarily travels along the first arm, which is sufficient for the MOT to work.

The MOT also contains the two necessary anti-parallel coils. The coils were built based on eq. (10) by choosing the parameters: N=80, L=8 cm, R=4.5 cm, I=3.3 A. This theoretically results in a B-field gradient of 10.2 G/cm. A measurement of the B-field between the coils was made by using a simple Gauss-meter. The error was high due to the imprecision of the Gauss-meter, but the measured gradient was approx. 9.6(6) G/cm. To build the coils, copper wire with a 0.52 mm^2 cross section was used, which has a recommenced current of 5 A [10]. This limit allows for a magnetic gradient of up to 15.44 G/cm, which is fine for the desired field gradient of approx. 10-15 G/cm.

After all the optical components were placed, two cameras were added as shown in fig. 7. One camera for continuous direct footage of the MOT, and another one for the actual data acquisition. Using the data aq. camera with a low gain, and an ND2-filter, the resulting image has very little background light, as the example in fig. 8. These images allow a user to calculate the radiated power of the MOT as a function of different parameters, as described in the data analysis. The MOT board is designed to have extra space in-between components to make it both more adjustable and more visually clear for new users.

3.4 Control panel and LabVIEW program

The setup is entirely controlled either by the laser control panel directly, e.g. for laser locking, or through a LabVIEW program, e.g. for turning on the magnetic field. The only exception is the power-supply for the dispensers, which has to be turned on manually.

The laser control panel shown in fig. 4, and more clearly in the appendix, is actually called a NIM bin, which holds a set NIM modules, that allows us to adjust e.g. the current, the phase for lasers, the AOM frequency. The control panel was already connected to the cooling laser and the repumper in the initial setup. I have since moved each NIM module around and swapped some of them out, to make the controls simpler to understand and more stable. The BNC cables have been swapped out for a tidier setup as well.

The LabVIEW program was built to control the the laser system, as well as the B-field and the main camera. Using Field Programmable Gate Arrays (FPGA's), both analogue and digital outputs and inputs were implemented, and connected to a breakout board. The breakout board was then connected to the control panel's NIM module for the AOM, a solid-state relay for the B-field, and directly to the camera for triggering. For future use, students can control the MOT and take measurements as saved images directly from a computer.

4 Data analysis

With control of different parameters of the MOT using LabVIEW, both static and dynamic measurements on the trapped atoms are possible. Four experiments were conducted to characterize the MOT, and each of them is presented in the following subsections. For each experiment, a set of images are taken. Using the Image module by PIL in Python, the images are converted to heat maps as shown in fig. 8.

(a) Direct image (b) Heat map

Figure 8: Both images are from a typical MOT measurement with a cooling laser powerof 100%, AOM freq. at 104 MHz, and a B-field with 3.3 A driving current. (a) Direct image of the MOT with a ND2-filter and low gain, and a ruler for scaling. The ruler is in millimetres. (b) Corresponding heat map made in Python, zoomed in and centered around the atomic cloud. The color is the bit intensity.

For each heat map a background measurement is subtracted, and then the bit intensity for each pixel is summed over, to get the total bit intensity of the MOT for that image. The bit intensity of the MOT, is in the following sections, referred to as the MOT intensity, and it is directly related to the radiated power of the trapped atoms. The MOT intensity is characterized as a function of different parameters. All data was acquired with an ND2-filter on the camera, low gain, and a short exposure time, to make sure the images did not saturate. Settings are specified for each of the four experiments.

4.1 Optimal settings for trapping

To characterize the MOT, the MOT intensity was measured as a function of different parameters: The AOM frequency, the cooling laser power, and the magnetic field. Optimal settings were determined for each parameter. For the magnetic field, it is specifically the optimal current for the coils that is determined. The laser power also changes, when the frequency of the AOM is adjusted. To account for this, the change in laser power as a function of AOM frequency was measured, and corrected for.

The settings for the these measurements were: Exposure time 8.08 ms, B-field current 3.6 A, AOM freq. 100 MHz, Cooling laser power 100% (controlled by the AOM). While measuring the affect of one of the parameters, that parameter varied as described by the following intervals. B-field: 0.4-4.4 A (steps of 0.2 A). Cooling laser power: 30%-100% (steps of 5%). AOM freq. 94-104.5 MHz (steps of 0.5 MHz). For each measurement the MOT was first turned off for 1 s and then turned on at the specific setting for 4 s.

4.2 Relative atom number

Another way of characterizing the MOT, is to determine the number of atoms being trapped. The total number of atoms trapped, N, can be measured, if the number of photons captured by the camera, N_{bit}, is converted to a total number of photons scattered, and divided by the scattering rate per atom.

For this conversion, the necessary parameters are the geometric factor S, the exposure time for the measurements τ, and the efficiency of the camera A. Here, a geometric constant, S, is necessary to relate the area of the camera's lens to the total surface of a sphere around the MOT, in which atoms are scattered. A converts the measured radiated power to the number of emitted photons. τ converts the rate to an absolute atom number. The total number of scattered photons is then

$$N = \frac{N_{bit}}{\tau \cdot A \cdot S} \frac{1}{R_{scatt}}. \tag{13}$$

This will in theory be the absolute atom number, but currently the efficiency of the camera is unknown. Instead, the relative atom number is determined. By defining a constant C for the product of parameters S, A, and τ, and by inserting the photon scattering rate from eq. (6) into eq. (13), it reduces to

$$N = \frac{N_{bit}}{C}\left(\frac{1 + I/I_{sat} + 4\delta^2/\Gamma^2}{I/I_{sat} \cdot \Gamma/2}\right). \tag{14}$$

By implementing a new constant C' equal to 1 over the denominator, the expression is further reduced to

$$N/C' = N_{bit}\left(1 + I/I_{sat} + 4\delta^2/\Gamma^2\right). \tag{15}$$

N/C' is referred to, as the relative atom number, and is a function of the detuning. In this experiment, for each chosen detuning, N_{bit} is measured, and the right hand side of eq. (15) is calculated. The measurements were conducted identically to the measurements for the optimal settings for the AOM frequency, except with an exposure time of 10.1064 ms, and a B-field current of 3.5 A.

4.3 Different repumper transitions

The effect of locking the repumper to different transitions was characterized as well. The MOT intensity was measured for different lock-points. The repumper was locked to $F = 1 \rightarrow F' = a$ transitions, with a being either zero, one, two, or one of the cross resonant lines in-between. However, we expect the $F = 1 \rightarrow F' = 0$ transition not to work, since an atom in the $F' = 0$ state can only decay back to $F = 1$ state, due to the dipole selection rules $\Delta F = 0, \pm 1$. Therefore, for this lock-point, the repumper cannot repopulate the $F = 2$ state, used by the cooling laser. As a result, the repumper can be locked to five transitions, but we only expect four of them to result in any trapping. The settings were: Exposure time 8.08 ms, B-field current 3.6 A, AOM freq. 100 MHz, and with varying repumper lock-points.

4.4 Temperature

A dynamic measurement was conducted to determine the temperature of the trapped atoms. Turning off the magnetic field and the cooling laser, the atoms where freely dissipating from the MOT. After a fixed time Δt, the MOT was illuminated with the cooling light at resonance, while leaving the magnetic field off. At that exact time, the camera took an image. From these images the velocity of the atoms can be determined and used to calculate the MOT's kinetic temperature.

Determining the speed and converting it to a temperature, can be done in different ways under different assumptions. The initial estimate for the temperature, as determined in this bachelor project, was measured and calculated as follows. For different Δt, the diameter of the atomic cloud was determined. The diameter in millimetres as a function of Δt, can then be fitted linearly, and the result is a velocity for the atomic cloud expansion, v_{exp}. Let $(u^2)_{avg}$ be the average over the squared velocities for each atom in the direction the diameter is measured. Under the assumption that $v_{exp}^2 = (u^2)_{avg}$, the average kinetic energy of the atomic cloud is $< E_{kin} >= 1/2m(u^2)_{avg} = 1/2mv_{exp}^2$. Assuming a Boltzmann distribution, the average kinetic energy of an atomic gas is equal to $1/2k_bT$ in each direction [8]. The change in diameter is an estimate for the velocity in one direction, so the temperature can, for these assumptions, be calculated as

$$T = \frac{v_{exp}^2 M}{k_b}, \tag{16}$$

where M is the atomic mass of rubidium-87 and k_b is Boltzmann's constant. For the temperature measurements, the AOM freq. was set to 101 MHz while trapping, and at 105.8 MHz (zero detuning) for 1 ms while illuminating the atoms. The Δt's are ranging from 0.5-2 ms (steps of 0.5 ms), with a camera exposure time of 4.07 ms, and B-field 3.5 A. The illumination time of 1 ms can be interpreted as the effective exposure time for these measurements. The ND2-filter was taken off the camera for these measurements.

5 Results & Discussion

The optimal settings are determined from different sets of measurements. Each data point is the mean of the intensities over two measurements (three for the AOM frequency), and the error is the associated SD (standard deviation). After calculating the mean and the error for each point, the data set was normalized to one, for each of the different parameters individually. These plots are shown in fig. 9. For each parameter, the setting resulting in the maximal MOT intensity was determined. The resulting optimal settings are shown in table 1. The uncertainties for the final values are determined from the span of data points near the maximum, which, within the errors on fig. 9, could be the actual maximum.

parameter	optimal setting
Current for B-field	3.4(2) A
AOM frequency	101.0(5) MHz
Cooling laser power	100(5)%

Table 1: Optimal settings for the highest MOT intensity. The results are the maximal values from fig. 9 for each parameter. The error is the span of data points which could be the actual maximum within the errors on fig. 9.

The results are as expected. The current for the B-field, allows for trapping within a wide range of currents, but there is an optimal setting. The optimal current for the field, results in a gradient of 10.5(6) G/cm, which is within the expected range of 10-15 G/cm. The AOM frequency results in a detuning of -9.7(10) MHz. For comparison, -10 MHz is the detuning found for the maximal number of trapped atoms in an article with a similar setup[11]. Assuming the detuning which maximizes the MOT intensity also maximizes the number of trapped atoms, the two results agree within the error. The cooling laser's power scales linearly with the MOT intensity, since the radiated power of the atoms scale with the power of the laser light, as expected. We expect a limit to this linearity, when the laser power becomes significantly high, but that is beyond the range of power used here. The errors on fig. 9 and in table 1, does not account for

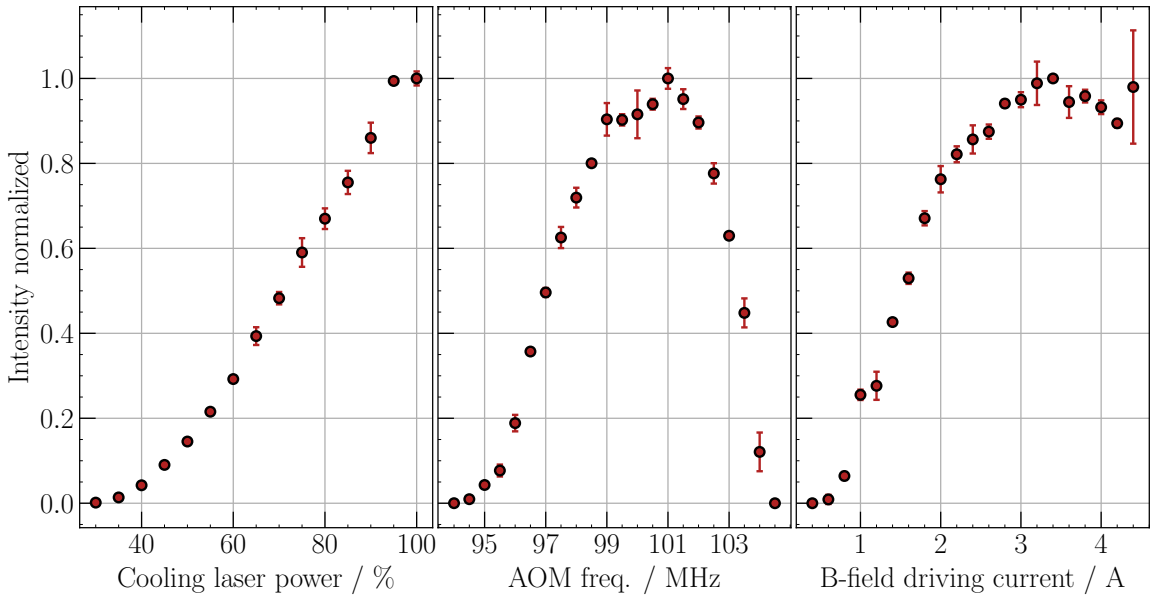

Figure 9: The MOT intensity normalized as a function of three different parameters: (left) the cooling laser power, controlled by the AOM. (middle) the AOM frequency. The laser detuning is near zero for 105 MHz. (right) the current of the B-field power supply, 3.4 A corresponds to a B-field gradient of -10.5 G/cm. Each data point is the mean over multiple measurements. Errors are the SDs for each calculated mean.

any systematic errors. A systematic error not accounted for, is that these parameters are not independent of one another, e.g. the B-field does effect the detuning of the atoms. To determine the absolute optimal settings, a higher dimensional plot of the correlations between the different parameters is recommended in the future.

The relative atom numbers as a function of detuning is shown in fig. 10. Each data point is again the mean of the intensities over two measurements, and the errors are the associated SDs. Note that this method, for estimating the errors, does not account for any systematic errors. Here, the data isn't normalized to one. This means that if future users of our setup calibrate the camera, they can use fig. 10 to determine the absolute atom number of the MOT. For such future reference, the maximum value measured was $N/C' = 1,306(7) \cdot 10^6$, with a detuning of approx. -11.75 MHz. The detuning is numerically approx. 2 MHz larger then the optimal detuning for the total atom number measured for a similar setup in [11]. This could relate to the chosen

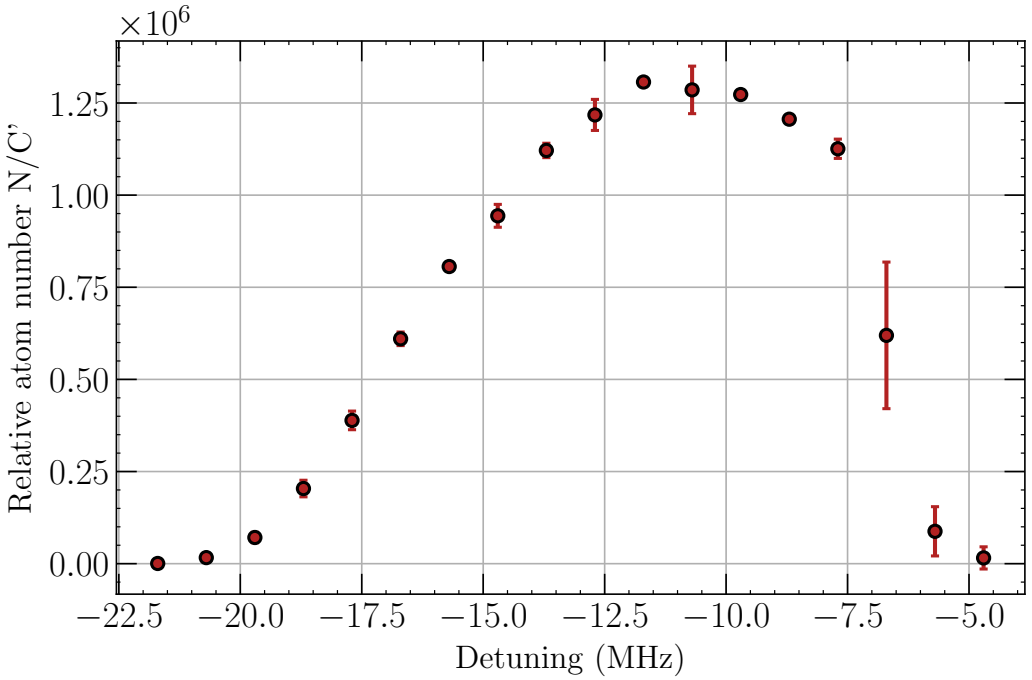

Figure 10: The relative atom numbers as a function of detuning, $\delta = \omega - \omega_0$. Each data point is the mean over two measurements. Errors are the SD for each calculated mean.

magnetic field strength for the measurements. Within our experiments, there is also a difference between the detuning resulting in the most trapped atoms, and the detuning resulting in the largest MOT intensity, since the total number of atoms, and the total radiated power of the atomic cloud is not linearly proportional. Some of the difference in these measurements, will also be a result of the slight change in magnetic field strength.

The repumper lock-points were examined by measuring the MOT intensity for each lock-point. The normalized results are shown in fig. 11. Each data point is the average over three runs, and the associated SDs are shown as the errorbars. Note that this method, for estimating the errors, does not account for any systematic errors.

As expected, the $F = 1 \rightarrow F' = 0$ had approx. zero intensity, but it isn't exactly zero. The MOT intensity for this lock-point, is still significantly higher than the background, even though it is near zero compared to the other lock-points. This is probably because a slight amount of the atoms have a velocity with a significantly

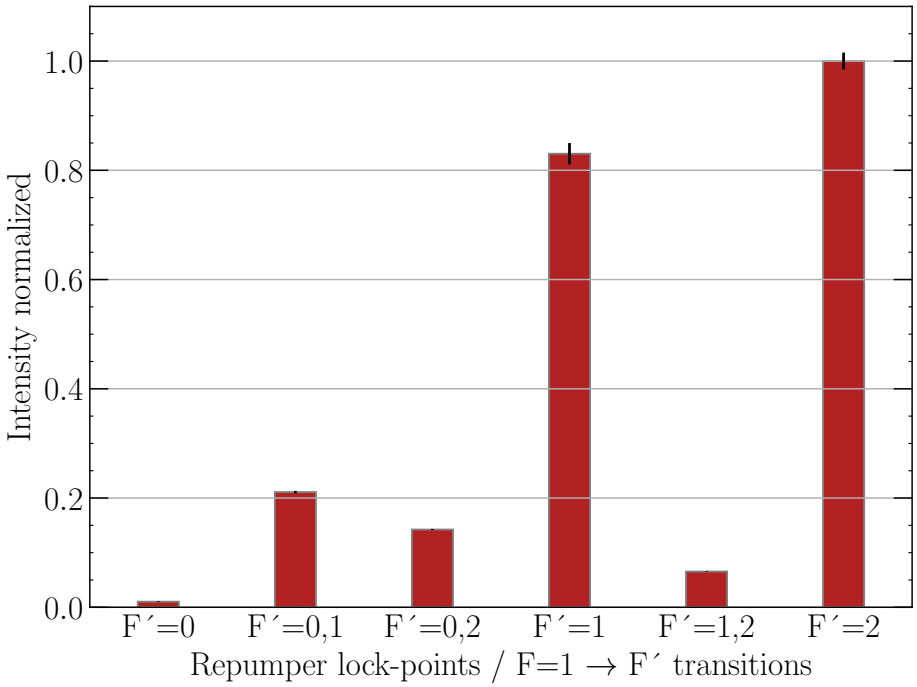

Figure 11: The MOT intensity normalized for different lock-points for the repumper, specifically different $F = 1 \rightarrow F' = a$ transitions, with a being 0, 1, 2 or one of the cross-resonant transitions from the saturated absorption spectroscopy. The intensity for each transition is the mean over three measurements. The error is the SD for each calculated mean.

large Doppler shift, such that the repumper can weakly excite the $F = 1 \rightarrow F' = 1$ transition. Thus, the MOT can trap a very small sample of atoms, resulting a low, but non-zero, MOT intensity.

Comparing fig. 3 (a) with fig. 11, the cross-resonant peaks are easy to lock to, but not the best for trapping. This makes sense, since the cross-resonant peaks are only a result of the saturated absorption spectroscopy, so when used for excitation directly, the frequency must be greatly Doppler shifted for these peaks to correlate with any of the three F' states. Therefore the repumper does not excite as many atoms, when locked to these cross-resonant lines. That the $F' = 2$ lock-point, has a higher MOT intensity then $F' = 1$, is a result of the relative decay rates. Atoms in the $F' = 2$ state has a higher probability of decaying to the $F = 2$ state, compared to atoms which are

excited to the $F' = 1$ state, so the repumper populates the $F = 2$ state faster when locked to the $F = 1 \rightarrow F' = 2$ transition.

The temperature was determined from a set of measurements with different Δt, as described in the previous section. Each Δt measurement was taken three times, and the diameter of the atomic cloud was determined and averaged for that specific Δt. The SDs were calculated as well. This yielded one final set of timestamps and atomic cloud diameters with errors, shown in fig. 12, which could then be used to calculate the approx. velocity of the trapped atoms after the MOT was turned off. The data was fitted to a linear fit, to determined the velocity, while accounting for the increase in error for larger timestamps. With the assumptions from section 4.4, the final temperature using eq. (16) is

$$0.10(5)\text{mK}. \tag{17}$$

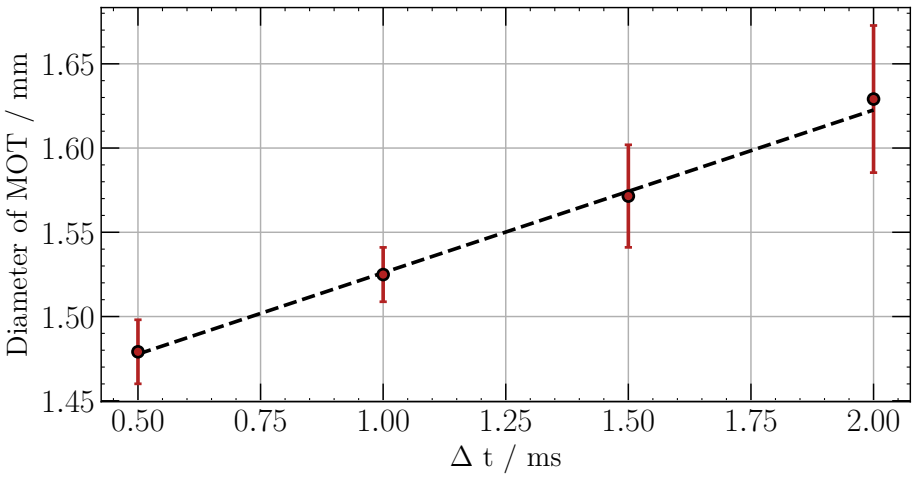

Figure 12: The MOT diameter as a function of time after the MOT was turned off, before it was illuminated by the cooling laser. Each data point is the average over three runs, with the errors being the SDs.

The uncertainty does not account for any systematic errors, such as the illumination time. The time we illuminate the atoms is 1 ms, which is of the same order of magnitude

as Δt, and so the images can not be seen as instantaneous. E.g. the image with Δt of 1ms, represents a measurement from 1 ms to 2 ms. The real velocity of the atoms is therefore lower than the fitted parameter, and the real temperature of the atoms, proportional to the velocity squared, is even lower still. However, since the Doppler cooling limit for rubidium-87 atoms is 0.146 mK, it stands to reason, that the real temperature of the atoms, would instead be above the determined temperature of 0.10(5) mK. Since, typically, it would not be expected that the atoms were cooled below the Doppler limit, with the precision of our setup. It is possible within the uncertainty, that the atoms have a temperature slightly above the Doppler limit, even for our measurements. In conclusion, the temperature should be further characterized in the future, by adjustments to the setup and additional measurements.

6 Conclusion

In this bachelor project a MOT has been constructed for cooling and trapping rubidium-87 atoms. To do so, a vacuum system with dispensers were built, along with two magnetic coils, and two optics setups. On the laser board, Doppler free spectra were achieved by saturated absorption spectroscopy for rubidium-87, for both the cooling laser and the repumper. The cooling laser traps the atoms using the $5S_{1/2} \rightarrow 5P_{3/2}$, $F = 2 \rightarrow F' = 3$ transition. The two lasers were connected to the MOT board were the rubidium atoms were trapped and cooled. Two cameras and a LabVIEW program were implemented for data acquisition and easy control.

Specifically, I designed, constructed and aligned the MOT optics board, including the magnetic coils, and adjusted the laser control panel to make laser locking easier. The fibre coupling, construction of the vacuum system and all data acquisition has been a collaboration between me and my lab-partner. For future use a user manual for the MOT is in the appendix.

The MOT has already, with relative ease, been used by other students to collect data, and so the MOT setup passed the test of being approachable. The MOT successfully

traps rubidium-87 atoms and cools them down to approx. 0.10(5) mK, as determined by a dynamic measurement of the dissipating atoms. This temperature estimate can be improved in the future, but is currently only a rough estimate. Static measurements were conducted to further characterize the MOT. The optimal settings for the MOT are shown in table 1, and can be used for future measurements. The maximal relative atom number of trapped atoms was $N/C' = 1,306(7) \cdot 10^6$ for a detuning of approx. -11.75 MHz.

6.1 Outlook

The following is a list of suggestions for future work.

A part of the data analysis could be implemented in the LabVIEW program as well, such that the total intensity and width of the MOT, is calculated in real time, and the output becomes a text file.

The mirror placed above the coils on the MOT board, and the associated $\lambda/4$ plate, are mounted to one of the posts for the coils. This was done to free up space in the setup and minimize the number of components. However, it means the coils cannot easily be moved, and therefore, it could be beneficial to change the mounting of the coils. It would allow users to test the effects of moving the coils, and make it easier to align the six laser beams' cross-point with the magnetic field center.

The maximal relative atom number can be converted by eq. (13) to an absolute atom number by calibrating the camera. The calibration will have to be done with the ND2-filter on the camera, as the filter was on doing the experiment.

With optimization of the setup, to improve the temperature estimate, the atomic cloud can be distinguishable from the background for higher time intervals Δt, allowing for more measurements. The time the atoms are illuminated by light, should also be decreased to significantly less then 1 ms, so the images can be interpreted as instantaneous. Realising these changes, should significantly improve the accuracy and the precision of the temperature estimate.

References

[1] Steven Chu. "Nobel Lecture: The manipulation of neutral particles". In: *Rev. Mod. Phys.* 70 (3 July 1998), pp. 685–706. DOI: 10.1103/RevModPhys.70.685.

[2] Jacob Johansen et al. "Fast Loading of a Trapped Ion Quantum Computer Using a 2D Magneto-Optical Trap". In: *2022 IEEE International Conference on Quantum Computing and Engineering (QCE)*. 2022, pp. 299–303.

[3] Daniel Adam Steck. ""Rubidium 87 D Line Data". Revision 2.1.4, 23 December 2010. URL: http://steck.us/alkalidata.

[4] CJ Foot. *Atomic physics*. Oxford University Press, USA, 2005.

[5] M. P. A. Jones. "Atom-Light Interactions". Course notes from The Univeristy of New Mexico. 2013. URL: http://info.phys.unm.edu/~ideutsch/Classes/Phys566F13/Notes%20from%20others/Atom-Light%20Interactions.pdf.

[6] C. Wieman, Gwenn Flowers, and Sarah Gilbert. "Inexpensive laser cooling and trapping experiment for undergraduate laboratories". In: *American Journal of Physics - AMER J PHYS* 63 (Apr. 1995), pp. 317–330. DOI: 10.1119/1.18072.

[7] Heather Lewandowski. "Coherences and correlations in an ultracold Bose gas". 2002.

[8] H.D. Young et al. *University Physics with Modern Physics*. Pearson, 2019. ISBN: 9781292314730. URL: https://books.google.dk/books?id=T7OoxgEACAAJ.

[9] O. Svelto. *Principles of Lasers, Fifth ed.* Springer US, 2010.

[10] *Cable Tester. Cable Wire Size and Current Capacity Rating Guide*. https://www.cable-tester.com/cable-wire-size-and-current-capacity-rating-guide/. Accessed: 30-05-2024.

[11] R. C. Das et al. "Narrow-line cooling of 87Rb using 5S1/2 → 6P3/2 open transition at 420 nm". 2022. URL: https://arxiv.org/pdf/2205.04054.

Appendix: User Manuel

With the control panel and the LabVIEW program, the MOT can easily be turned on, and used for experiments. In the following, is a detailed description for how to operate the MOT, including the laser locking and the essential parameters used.

To realise a MOT, the dispensers have to be turned on manually with the small power-supply next to the laser control panel. The current for the dispensers should be set between $2.2 - 2.4$ A. Lock the lasers as described below. Then, using the LabVIEW code, turn on the magnetic field. The B-field should power-supply should never be run above 5 A. With the LabVIEW interface, turn on the AOM. Use AOM power of 100%, corresponding to maximal cooling laser power, and set an AOM freq. within $100MHz \pm 5$ MHz. To take and save the images, a second LabVIEW program is opened, that can either run continuously, or have a trigger. Here, you can specify a folder on the computer and a file name for each measurement. Currently, all data analysis is done separately in Python.

Laser locking

To actually lock the lasers, the laser control panel, shown in fig. A1, and the two oscilloscopes are needed. The bottom scope is for the cooling laser, and the top scope is for the repumper. On both oscilloscopes, the inputs have the same colors, e.g. the purple signal is the error signal on both.

On the control panel, everything to the left concerns to the repumper. The only necessary variables for locking the repumper is the sweep gain, the current and the phase. Using the current, and the phase you should be able to find the right set of peaks, (a) in fig. 3. Sweeping in using the sweep gain, you essentially limit the range of frequencies the laser is sweeping over, until only the specific peak needed is within range on the oscilloscope. If the error-signal is not crossing zero right at the peak, it is necessary to adjust the pound-driver phase for the repumper. When centered on the

peak, flick the lock switch, to lock the repumper to that specific frequency. If on the scope, the lock point is placed differently than where the top of the peak was before, the laser has locked to a wrong peak, and you need to repeat the process once more.

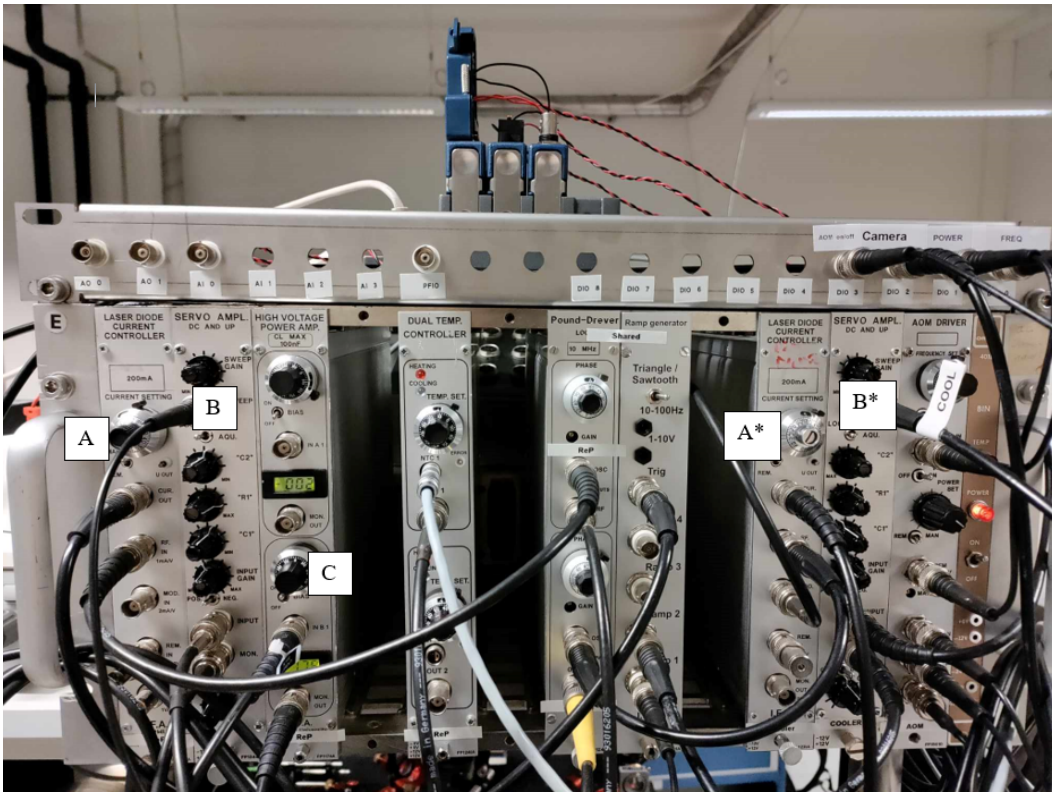

Figure A1: Control panel for the lasers. A: current control for the repumper. B: sweep gain above and lock switch below, for the repumper. C: phase knob for the repumper. A*: current control for the cooler. B*: sweep gain above and lock switch below, for the cooler.

The same procedure holds for the cooling laser, where all relevant panels are to the right. The cooler is much more stable and typically doesn't need much adjusting. Here, only the current is relevant for finding the right peak, then simply sweep in and flick the lock switch.

We lock the cooling laser to the $F = 2 \rightarrow F' = 1, 3$ cross-resonant line, the arrow on fig. 3 (b). This frequency is 211.7 MHz below the $F = 2 \rightarrow F' = 3$, which can be calculated directly from fig. 1. Afterwards the laser is sent through an AOM twice, which increases the frequency of the cooling laser by approx. 100 ± 5 MHz each time.

The laser ends up being slightly detuned from the $F = 2 \rightarrow F' = 3$ line by approx. $\delta = 12 \pm 10$ MHz. The repumper is locked to the $F = 1 \rightarrow F' = 2$ transition, the arrow on fig. 3 (a). The repumper does not need to be detuned from this value, since the MOT works even with a low efficiency for the repumper. The resulting laser frequencies are then the transitions initially drawn on fig. 1 in section 2.1. The sample of rubidium, used in both the experiment and in the samples for the spectroscopy, does contain both rubidium-87 and rubidium-85, due to the natural abundance of both isotopes. Here, rubidium-87 is used, and therefore everything in this project has been described with that isotope, but it is relevant to know for the laser locking that rubidium-85 can be seen in the spectra as well. If a laser has moved significantly, you might see the saturated absorption spectrum for a set of peaks not shown on fig. 3. This can be one of two sets of rubidium-85 peaks, which have frequencies in-between the two sets of rubidium-87 peaks. Turning the current knob will change the laser frequency until the oscilloscope once again shows the preferred set of peaks.